Implication of Illumination Beam Geometry on Stray Light and Bandpass Characteristics of Diode Array Spectrometer

Joel Kuusk, Ilmar Ansko, Agnieszka Bialek, Riho Vendt, and Nigel Fox

***Abstract*—This paper describes spectral stray light measurements of diode array spectrometers and, in particular, the dependence of stray light and bandpass properties on the illumination beam geometry. The effects of underfilling and overfilling the nominal field of view of the instrument are presented. Our measurements showed that the line spread function of a commercially available miniature spectrometer module having a fiber optic entrance with 0.22 nominal numerical aperture can depend on fiber illumination cone apex angle up to $40°$, which is well above the $25°$ nominal acceptance cone apex angle of the fiber. The bandpass width and amount of stray light inside the spectrometer increased proportionally with the illumination cone angle. Spectral stray light measurements with different setups gave consistent and repeatable results for similar illumination geometries. Care should be taken to ensure that illumination geometry during spectral stray light characterization of a spectrometer matches the conditions during target measurements for which the spectral stray light corrections are applied. The impact of illumination geometry during stray light characterization depends on the target signal and particular application. Photochemical reflectance index (PRI) and normalized difference vegetation index (NDVI) of a hemiboreal birch forest are used as contrasting examples in this paper. Compared to natural variability, the relative impact on PRI exceeds that of NDVI by 10 times.**

***Index Terms*—Optical fiber devices, optical spectroscopy.**

I. Introduction

In FIELD spectroscopy and remote sensing applications, diode array spectrometers have become rather common. They present several advantages over scanning double monochromator systems such as compact size, lack of moving elements, relatively low cost, and simultaneous acquisition of all the spectral bands, which significantly improves the measurement speed. In addition, diode array spectrometer modules can be fairly easily integrated into custom-designed instruments. All these properties make diode array spectrometers especially suitable for rapidly expanding unmanned aerial vehicle (UAV) applications, as well as for already well-established field measurements for "ground truth" type activities related to validation of satellite sensors. One of the main limitations of diode array spectrometers, however, is their relatively high internal spectral stray light level [1]. If the optical input of a spectrometer is illuminated with monochromatic radiation, in an ideal case, a signal should be recorded only by the corresponding spectral band of the instrument. Due to imperfections of the dispersing element, internal reflections, and several other reasons, some light is always scattered inside real instruments and incorrectly recorded by sensor elements corresponding to other spectral bands. Such incorrectly recorded signal is called spectral stray light. While the spectral stray light levels of high-quality double monochromators can be below 10^{-8} [2], compact diode array spectrometers perform much worse and even high-quality instruments have spectral stray light levels around 10^{-5} in the case of monochromatic source or 10^{-3} when measuring a broadband source [3]. The stray light levels can be even two orders of magnitude higher [2], [3] for poor quality instruments, meaning they are likely to be inadequate for applications where low-intensity spectral components of a broadband source have to be measured [3], [4].

When a monochromatic source is measured with an array spectrometer, the recorded signal (for each pixel) normalized by the maximum value is called the spectral line spread function (LSF) [3]. The LSF describes the relative signal generated by each element of the detector array when excited by monochromatic radiation at a particular wavelength. LSFs measured with monochromatic sources corresponding to central wavelengths of every pixel of the spectrometer form a spectral stray light matrix (SLM). Columns of the SLM are LSFs, rows of the SLM are slit-scattering functions (SSF) [2], which describe the relative spectral responsivities of each individual element of the detector array. The value recorded by a single pixel of the spectrometer is a convolution of the input optical spectral power distribution and the SSF associated with that pixel. When

Manuscript received December 15, 2017; revised April 6, 2018 and May 17, 2018; accepted May 23, 2018. Date of publication June 19, 2018; date of current version August 21, 2018. This paper was supported in part by the Estonian Ministry of Education and Research (Project SF0180009Bs11) and in part by the European Space Agency (MERIS Validation Team). The STAIRS measurements were supported by the European Union and European Metrology Research Programme through the European Metrology for Earth Observation and Climate Joint Research Project (MetEOC2). The EMRP is jointly funded by the EMRP participating countries within EURAMET and the EU. The Zeiss MMS 1 module used in this paper is a part of the SMEAR Estonia (Station for Measuring Ecosystem–Atmosphere Relations) infrastructure, funded by the European Commission through the European Regional Development Fund (Estonian Research Infrastructures Roadmap project Estonian Environmental Observatory (3.2.0304.11-0395)). *(Corresponding author: Joel Kuusk.)*

J. Kuusk, I. Ansko, and R. Vendt are with the Tartu Observatory, University of Tartu, Tõravere 61602, Estonia (e-mail: joel.kuusk@ut.ee; joc@sputnik.aai.ee; riho.vendt@ut.ee).

A. Bialek and N. Fox are with the Earth Observation, Climate and Optical Group, National Physical Laboratory, London TW11 0LW, U.K. (e-mail: agnieszka.bialek@npl.co.uk; nigel.fox@npl.co.uk).

Color versions of one or more of the figures in this paper are available online at http://ieeexplore.ieee.org.

Digital Object Identifier 10.1109/JSTARS.2018.2841772

the SLM of a spectrometer is known, the contribution of stray light can be removed from the output signal and the input optical signal can be restored. This can be done by a mathematical operation called deconvolution. From literature, several deconvolution algorithms can be found, based on either an iterative approach [2], [5], [6] or inverse matrix multiplication [3], [7].

Thus, in order to remove the stray light contribution by deconvolution, a knowledge of the spectrometer SLM is necessary. To measure the LSFs, a monochromatic source is required, either from tunable lasers [2], [3], [6], [7] or from a double monochromator [8], [9]. Some authors have also reported successful attempts to measure LSFs with only a few monochromatic sources and modelling [10]–[12] or interpolating [13] the rest of the LSFs. However, almost no information can be found in the literature regarding the influence of the optical setup on the measured LSFs. The importance of illumination beam geometry and input optics has been only briefly mentioned [7], [14], [15]. At the same time, it is known that the responsivity of a spectrometer may depend on the direction of the incident flux [2], [16]. In this paper, we present a case study based on a class of commercial spectrometer modules with fiber optic input, and show how illumination geometry can affect the measured LSFs.

In Section II, we present measurements of LSFs using both a tunable laser and a monochromator system and report the results of LSFs of a Zeiss MMS 1 (Monolithic Miniature Spectrometer 1). The LSFs were measured with different illumination geometries applying a tunable laser, and the results were verified by using a double monochromator. While a Zeiss MMS 1 is utilized as the core of several remote sensing instruments, the optical fiber is usually coupled with additional optical element such as a lens or a cosine response diffuser. We therefore also measured the LSFs of two TriOS RAMSES (radiation measurement sensor with enhanced spectral resolution) spectrometers to study how integrated foreoptics affect the impact of illumination geometry. The RAMSES measurements are presented in Section III. We conclude with a discussion of the significance of our findings for spectral stray light characterization and an example of possible impact on remotely sensed data products such as photochemical reflectance index (PRI) and normalized difference vegetation index (NDVI).

II. Spectral Stray Light of a Zeiss MMS 1

This part of our investigation used a miniature spectrometer module type MMS 1 by Carl Zeiss (Jena, Germany). The Zeiss MMS 1 is a compact and robust miniature spectrometer module with no moving parts. It is designed for the visible and near-infrared (NIR) spectral region and is available in two variants: The standard version has a Hamamatsu S3904-256Q silicon photodiode array detector, whereas a Hamamatsu S8381-256Q array is used in the enhanced NIR sensitivity variant. Both of these detectors are manufactured using N-type metal-oxide-semiconductor technology. The optical input is a permanently attached 24 cm-long fiber optic bundle with a so-called cross-section converter—the fibers in the bundle are aligned inside the spectrometer to form the input slit of the spectrograph. According to the product data sheet, the bundle consists of approximately 30 quartz glass fibers, each having 70 μm core diameter and 0.22 numerical aperture (NA); therefore, the apex angle of the nominal fiber acceptance cone is approximately 25°. A concave holographic grating is simultaneously used as a dispersive and imaging element. The cross-section converter, the imaging grating, and the diode array sensor are attached to a solid glass core. A preamplifier is integrated in the MMS 1 module, but additional electronics are needed to operate the device. In this paper, an polytetrafluoroethylene (FEE)–HS front-end electronics unit manufactured by tec5 AG (Oberursel, Germany) was used as an analog-to-digital converter (ADC). Integration time control and data acquisition are handled by custom designed electronics and software. The Zeiss MMS 1 has 10 nm spectral resolution and 3.3 nm spectral interval. The 256 pixels of the sensor array cover the spectral range from 306 to 1140 nm.

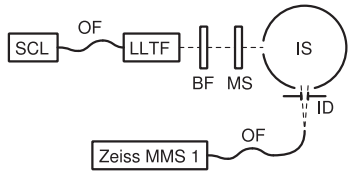

Fig. 1. Spectral stray light measurement setup using the STAIRS. SCL—supercontinuum laser, OF—optical fiber, LLTF—laser line tunable filter, BF—blocking filter, MS—mechanical shutter, IS—integrating sphere, and ID—iris diaphragm.

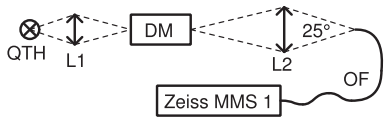

Fig. 2. Spectral stray light measurement setup using a double monochromator. QTH—quartz-tungsten-halogen light source, L1 and L2—condenser lenses, DM—double monochromator, OF—optical fiber of the MMS 1.

The MMS 1 spectrometer module (NIR enhanced variant), FEE–HS front-end electronics, and interface electronics used in this study are components of the SkySpec B hyperspectral radiometer described in [17]. As mentioned, the LSFs were measured with a spectrally tunable absolute irradiance and radiance source (STAIRS) [18] and verified with a double monochromator setup.

A. STAIRS Measurements

Fig. 1 shows the STAIRS measurement setup. STAIRS is based on a supercontinuum laser and a laser line tunable filter (LLTF) [18]. Broadband radiation from the supercontinuum laser is coupled into the LLTF, which is essentially a monochromator based on a volume Bragg grating. A glass-blocking filter must be used for suppression of second-order diffraction signal for LLTF wavelength settings above 790 nm. The full-width at half maximum (FWHM) of the output radiation from the LLTF varies with wavelength and is generally below 2 nm, which is one-fifth of the spectral resolution of the Zeiss MMS 1. In this experiment, STAIRS can therefore be considered a monochromatic source. Stray light characterization involves measurement of extremely weak signals; therefore, accurate knowledge of dark signal is essential. Since MMS 1 does not have an

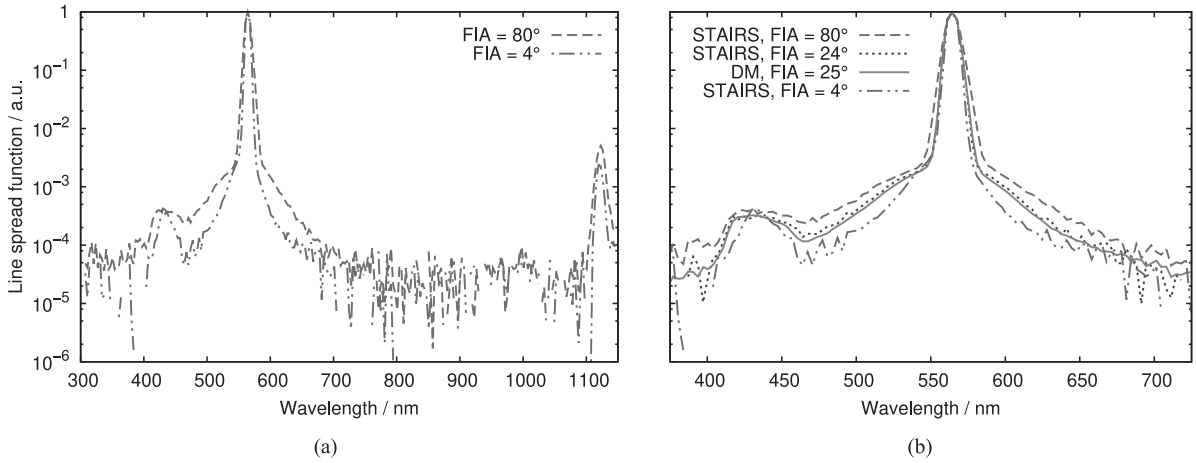

Fig. 3. LSF of Zeiss MMS 1 measured with 564 nm monochromatic input at different illumination geometries. Dashed lines are STAIRS measurements, and solid line is a double monochromator measurement. (a) Entire spectral scale of MMS 1. (b) LSF around the central maximum.

internal shutter or masked pixels, an external shutter is needed for collecting dark signal readings.

In this investigation, the monochromatic output of STAIRS was coupled to an integrating sphere and the input fiber of the MMS 1 module was pointed at the output port of the sphere. This ensured that the field of view (FOV) of the fiber was uniformly filled. An iris diaphragm (adjustable from 1 mm to 10 mm diameter) was placed between the fiber and the integrating sphere. The distance between the fiber and diaphragm was chosen so that a 6.4-mm diameter of the diaphragm corresponded to the nominal acceptance cone of the fiber. The fiber illumination cone apex angle (FIA) varied from 4° to 39°, so allowing both underfilling and overfilling of the acceptance cone of the fiber, while still maintaining the uniformity of light within the illuminated cone. When the diaphragm was removed and the fiber placed directly in front of the exit port of the sphere, the FIA was limited to approximately 80° by the edge of the sphere port.

During measurements, the laser power setting was fixed and other computer-controlled components (LLTF, shutter, spectrometer) of the measurement setup were managed using custom software. First, for each detector element of the Zeiss MMS 1, the LLTF was tuned to a wavelength setting corresponding to its nominal central wavelength. Second, the integration time of the spectrometer was adjusted so that the maximum signal recorded from this pixel was between 60% and 90% of the dynamic range. Then, the LLTF was iteratively fine-tuned, until the signals recorded from the pixels on either side of the central maximum differed from each other by less than 3% of the signal recorded from the central pixel; this procedure ensured that the true central wavelength of the pixel was found. Finally, the output from all pixels of the array was averaged for 1 s or 10 acquisitions, whichever was longer, when illuminated by the monochromatic radiation from STAIRS (i.e., light signal) and with the external shutter closed (i.e., dark signal). The LSF was calculated as the light signal for each pixel minus the corresponding dark signal. The LLTF was then tuned to the nominal central wavelength of the next pixel and the whole process was repeated. The spectral range of the Zeiss MMS 1 exceeds the capabilities of the STAIRS system; thus, only a subset of LSFs were measured, corresponding to 500–930 nm monochromatic inputs.

B. Double Monochromator Measurements

The double monochromator setup is depicted in Fig. 2. In this setup, the broadband illumination from a 55 W quartz-tungsten-halogen lamp was projected using the convex lens L1 onto the input slit of a Bentham DTMS300 double monochromator. The diameter and position of the lens L1 were matched with the F/4.1 aperture of the monochromator. The DTMS300 is completely computer controlled and includes a shutter and a filter wheel with order sorting filters. The slits of the monochromator were adjusted to provide monochromatic output with 1 nm FWHM bandwidth. The integrating sphere could not be used in this setup because the output power of the double monochromator system is much lower than the STAIRS and the light collecting surface area of the fiber is very small. Thus, the output from the monochromator was coupled to the fiber using the condenser lens L2, which imaged the output slit of the monochromator onto the end of the fiber and was positioned so as to gather all the output radiation from the monochromator maximizing the coupling efficiency. The lens was chosen so that the radiation from the monochromator approximately filled the nominal acceptance cone of the fiber; however, given the fact that the slit is rectangular, it was not possible to fill the acceptance cone of the fiber completely. The double monochromator setup covered the whole spectral range of the Zeiss MMS 1 spectrometer module.

C. Results

Fig. 3 presents the Zeiss MMS 1 LSFs corresponding to 564 nm monochromatic input measured with different illumination geometries. It is clearly visible that the main stray light features are comparable for all geometries, but the absolute level of stray light depends on the FIA during the measurement. A complete SLM measured with the double monochromator setup is presented in Fig. 4. Several stray light features are distinguishable, such as broadening of the central maximum, additional maxima caused by internal reflections, and second-order

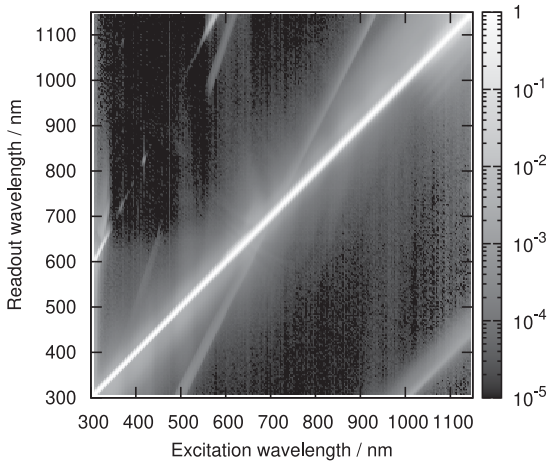

Fig. 4. Spectral SLM of the Zeiss MMS 1 spectrometer module. Each column is one acquired LSF. All the features apart from the one-to-one diagonal can be considered spectral stray light.

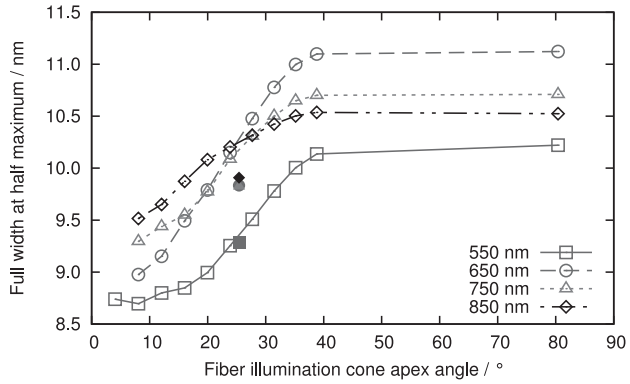

Fig. 5. FWHM of central maximum of LSF for different excitation wavelengths. Empty symbols connected with a line are STAIRS measurements, and filled symbols are double monochromator measurements.

diffraction, which is not completely blocked by the higher order blocking filter coated directly onto the sensor. The FWHM of the central maximum is shown in Fig. 5 for four excitation wavelengths. The actual width of central maximum changes with the excitation wavelength; however, its dependence on FIA is visible up to 40° and is similar for all LSFs measured. An increase of FIA by 1° causes an increase in FWHM by 0.4%–0.8%. The FWHM as a function of wavelength for different illumination geometries is presented in Fig. 6. Although the FWHM value varies with the illumination geometry, an increase of FWHM with wavelength is visible for all data series shown in Fig. 6, and this increase is more rapid in the NIR spectral region. In addition, a local widening of the central peak of the LSF around 630 nm is visible for all illumination geometries.

The amount of stray light inside a spectrometer can be quantified by the proportion of the total recorded monochromatic signal, which is contained within the central peak; the higher this proportion, the lower the stray light. The fraction of the total signal contained within the five central pixels around the maximum of the LSF is plotted in Fig. 7. Increasing the FIA by 1° increases the amount of stray light inside the MMS 1

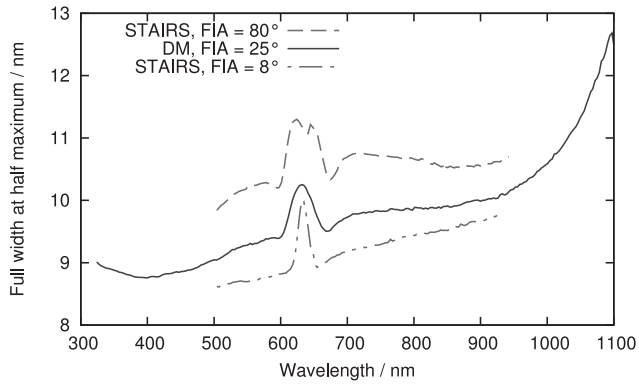

Fig. 6. FWHM of central maximum of LSF measured at different illumination geometries.

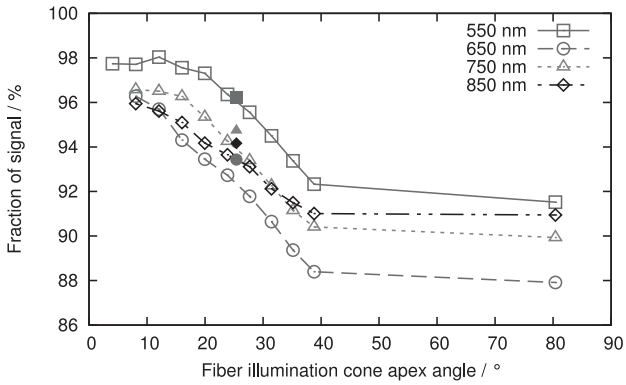

Fig. 7. Fraction of measured signal inside the central maximum of the LSF for different excitation wavelengths. Empty symbols connected with a line are STAIRS measurements, and filled symbols are double monochromator measurements.

and decreases the fraction of signal inside the central peak by 0.2%–0.3%.

III. Spectral Stray Light of RAMSES Spectrometers

To evaluate the impact of the fore-optics on the stray light characterization at varying illumination geometries, a set of ad-hoc measurements was performed with two commercial TriOS RAMSES spectrometers, namely one radiance and one irradiance units. The TriOS RAMSES family of spectrometers is designed for water remote sensing applications and are widely used for above-water as well as in-water measurements. These are highly integrated devices comprised of a Zeiss MMS 1 spectrometer module, ADC and interface electronics, and input optics, all packaged in a water-tight housing. Unlike the standard MMS 1 module, the sensor of RAMSES spectrometer has masked pixels that can be used for estimation of dark signal without a mechanical shutter. The dark signal pattern is characterized in the factory and scaled for each target measurement based on the signal from the masked pixels [19]. The irradiance sensor (model RAMSES ACC–VIS) has a cosine response diffuser mounted in front of the fiber optic input of the MMS 1. In the radiance spectrometer (model RAMSES ARC–VIS), a lens is used to define a 7° FOV. As for the characterization of MMS 1, measurements were performed with the STAIRS

tunable laser and verified with the monochromator. In addition, specific measurements were carried out with an HeNe laser applied to the RAMSES ACC irradiance unit to assess the effect of underfilling/overfilling the sensor diffuser.

A. STAIRS Measurements

The STAIRS measurement setup for the RAMSES instruments was similar to that used for the Zeiss MMS 1 measurements depicted in Fig. 1, but the mechanical shutter and iris diaphragm were not used and both instruments were measured in the overfilled FOV condition. The STAIRS wavelength fine-tuning was carried out as described in Section II-A. To obtain the LSF, 12 measurements were recorded in the unsaturated condition, followed by 12 saturated measurements using 16 times longer integration time. The LSF was obtained by combining the saturated and nonsaturated measurements in order to increase the dynamic range. This method is called bracketing [3], [4], [13]. Specifically, pixels from the saturated measurements for which the value was less than half the saturation level were used in the LSF, coupled with data from the nonsaturated measurements for other pixels (with appropriate scaling applied in these cases).

B. Double Monochromator Measurements

The integration time of RAMSES instruments can be selected from 12 predetermined settings in the range of 4–8192 ms. However, even at the longest setting, the measured signal in the ultraviolet (UV) spectral region is very small for an incandescent source. Therefore, a 450-W xenon short arc lamp in a Newport 66923 lamp housing (with integrated condensing optics) was used as a light source in the double monochromator setup. In order to avoid damaging the order sorting filters and gratings of the double monochromator, a Newport 6214 distilled water filter was used for blocking the short-wave infrared radiation outside the spectral range of the RAMSES spectrometer, and the lamp was slightly defocused.

Three different double monochromator setups were used to characterize the stray light of the two RAMSES instruments. Initially, the RAMSES spectrometer was placed directly behind the exit slit of the monochromator. The measurements were then repeated with a 0.4 mm-thick layer of sandpaper-roughened PTFE placed between the monochromator and the spectrometer. Finally, the monochromatic radiation from the double monochromator was passed through an integrating sphere before reaching the entrance optics of the spectrometer.

C. HeNe Laser Measurements

Additional measurements with an HeNe laser were performed with the irradiance unit, in order to test how underfilling or overfilling the diffuser surface area influences the measurement results. The 0.7-mm diameter beam of a Thorlabs HRS015 laser was aligned with the optical axis of the 7-mm diffuser and the signal was recorded. Then, the beam was passed through an integrating sphere to overfill the diffuser area and the measurement was repeated.

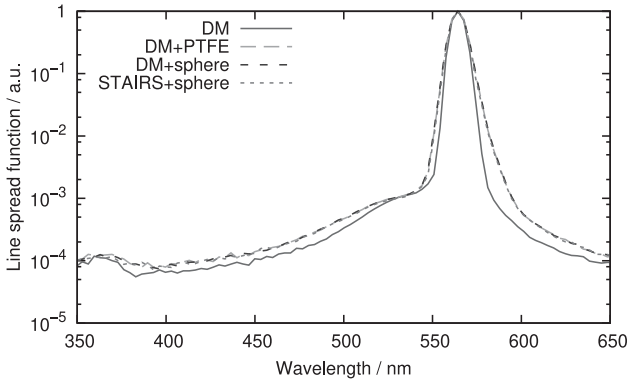

Fig. 8. Central part of the LSF of RAMSES ARC–VIS radiance spectrometer at 564 nm monochromatic input measured with four different setups. All the dashed lines are on top of each other.

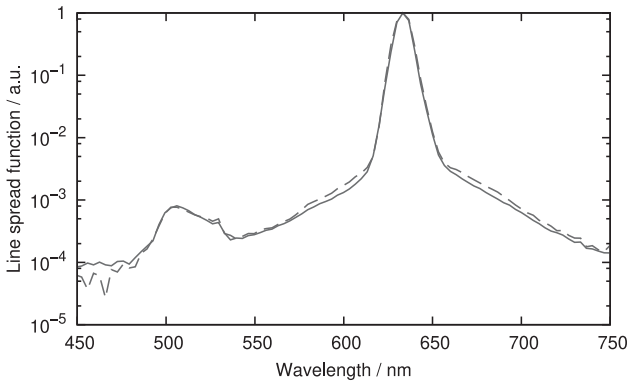

Fig. 9. Central part of the LSF of RAMSES ACC–VIS irradiance spectrometer using 632.8 nm monochromatic input from an HeNe laser. Solid line—narrow laser beam, dashed line—diffuser overfilled.

D. Results

The LSFs of the radiance unit measured with the four different setups and applying 564 nm as excitation wavelength are shown in Fig. 8. The STAIRS measurements closely match the double monochromator measurements carried out with the integrating sphere or the layer of PTFE. Results obtained with the spectrometer pointed directly to the exit slit of the monochromator, instead, exhibit narrower central peak and lower level wings. Compared to the LSF of the Zeiss MMS 1 module described in Section II and presented in Fig. 3, the internal reflection peak is shifted toward shorter wavelengths and is located below 400 nm.

Apart from the measurement noise, equivalent LSFs were obtained with the irradiance unit, regardless the measurement setup. Remarkably, adding an integrating sphere or a layer of PTFE between the monochromator and RAMSES did not change the shape of the measured LSFs.

Finally, results obtained with the irradiance unit applying the HeNe laser are plotted in Fig. 9. Compared to the results measured with a narrow laser beam, overfilling the diffuser surface slightly raised the wings of the LSF and increased the FWHM of the central peak by 0.7 nm.

IV. Discussion

There are several interesting aspects related to the spectral stray light test results presented in the preceding sections. First, a continuous increase of the stray light signal with the increase of the illumination cone angle, beyond the point of fully filled acceptance angle of the fiber, was observed. From Figs. 5–7, it is evident that stray light properties of the MMS 1 spectrometer module change with increase of the FIA. However, these changes do not stop when the nominal fiber acceptance angle is completely filled; they still continue for overfilled acceptance angles up to value as high as 40° and then reach a plateau. It is important to remember that the NA of a fiber describes the maximum angle where total internal reflection is possible between the core and cladding of the fiber, enabling propagation of guided modes. At greater incidence angles, some of the light escapes through the cladding and is absorbed by the coating of the fiber, thus, attenuating the radiation propagated along the fiber. The total attenuation is related to the number of internal reflections, i.e., the length of the fiber. As the length of the fiber of Zeiss MMS 1 is only 24 cm, the light entering the fiber outside the nominal acceptance cone is not completely attenuated and reaches the spectrometer, so influencing the stray light properties. Additional tests were performed to measure the nominal NA of the Zeiss MMS 1 fiber. For this purpose, the fiber input end was tilted in front of a red diode laser. The tests confirmed that the NA of this fiber is 0.22, but attenuation outside the acceptance cone is not very strong. At 20° incidence angle (i.e., corresponding to 40° FIA), the signal level was 2% compared to the normal incidence signal. When a 25 m-long extension fiber was added, the 2% signal level was reached at 15.5° incidence angle.

Second, a clear difference was seen between the STAIRS and double monochromator test results. Neither the double monochromator nor the STAIRS system provides truly monochromatic radiation. The FWHM of the STAIRS output radiation is about 1.1 nm for wavelength settings below 600 nm, which matches rather closely the 1 nm FWHM of the double monochromator but increases at longer wavelengths reaching 2 nm at 850 nm [18]. This could explain the difference between the double monochromator and STAIRS measurements visible in Figs. 5 and 7. To test this hypothesis, the stray light measurement was repeated with the monochromator set to 550 nm with a bandwidth of 2 nm FWHM. It was found that this increase of the FWHM by 1 nm had no significant effect on the recorded LSF. Assuming the same behavior for all the wavelengths, the 1 nm discrepancy in FWHM between the two systems for wavelengths above 600 nm could not cause the difference in the test results.

Thus, the nonuniformity of radial intensity distribution at the exit of the fiber during the double monochromator measurements was examined. The fiber of the MMS 1 was replaced with a fiber optic patch cord and the other end of the patch cord was pointed toward a white surface. It was seen that the central area of the circular image on this surface was brighter than the outer part. The central area corresponds to smaller incidence angles, which have lower stray light contribution according to Fig. 7. As the distribution of energy inside the fiber illumination cone is biased toward smaller incidence angles in the double monochromator tests, the stray light levels are lower compared to the STAIRS tests performed at the same FIA values (see Figs. 5 and 7).

Finally, the tests revealed a sudden change in the FWHM of central maximum of the LSF in one particular spectral region. In Fig. 6, a local widening of the central peak of the LSF is visible around 630 nm. The exact cause of this widening is unknown but a plausible explanation could be refraction of light from the edge of the higher order blocking filter that is coated onto the detector array. Since only the second-order diffraction needs to be blocked and first-order diffraction must reach the sensor, the higher order blocking filter must start from the middle of the sensor array and cover only the pixels corresponding to longer wavelength spectral bands. The edge of this filter coating can cause some refraction of light, which results in the widening of the spectral line on the surface of the sensor array. This nonmonotonic behavior of FWHM as a function of wavelength also explains the order of lines in Fig. 5.

End-users generally prefer to use commercially available self-contained spectrometers rather than custom-designed instruments. TriOS RAMSES-series spectrometers were therefore used in this study to check whether spectrometers with integrated optics have similar stray light characteristics to those observed for the underlying spectrometer modules with a bare fiber input. Fig. 8 shows that the general trend is similar. A RAMSES ARC–VIS radiance sensor with 7° full-angle FOV placed directly behind the exit slit of a monochromator recorded a narrower LSF than that measured using the same instrument when the monochromator output was passed through an integrating sphere. Radiation from the integrating sphere significantly overfills both the entrance aperture and FOV of the RAMSES radiance spectrometer. This is comparable to a common real-life measurement setup, where the instrument is used for measuring radiance of the sky or water surface. Similar results to those with the integrating sphere were obtained when a 0.4 mm-thick layer of sandpaper-roughened PTFE was placed between the monochromator and RAMSES spectrometer. The layer of PTFE diffuses the incident radiation and overfills the FOV of the spectrometer. The RAMSES ACC–VIS irradiance spectrometer has an integrated diffuser that acts in a similar manner, with the result that in the double monochromator experiments for this instrument the shape of the measured LSF was found not to depend on illumination geometry, apart from an extreme condition such as illuminating the diffuser with a narrow laser beam. In this case, the integrated diffuser of the RAMSES ACC–VIS cannot completely disperse the laser beam energy, thus, the radiance of the diffuser surface inside the instrument and in the FOV of the fiber of the MMS 1 spectrometer module remains slightly nonuniform, which affects the recorded LSF (see Fig. 9). This suggests that underfilling the diffuser surface during stray light characterization may lead to underestimation of spectral stray light.

A. Possible Impact on Data Products

The impact of spectral stray light correction on the actual target measurements depends on the spectral composition of the target signal and the specific use case. As an example, the effect

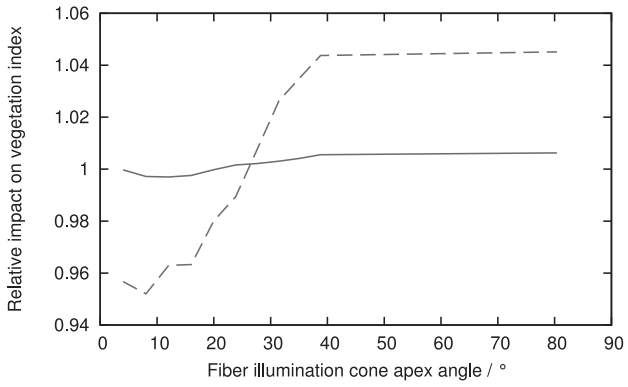

Fig. 10. Example of possible impact on commonly used vegetation indices NDVI (solid line) and PRI (dashed line) for hemiboreal birch stands.

is demonstrated for two commonly used vegetation indices: PRI and NDVI, which are defined as

$$\mathrm{PRI} = \frac{\rho_{531} - \rho_{570}}{\rho_{531} + \rho_{570}} \tag{1}$$

and

$$\mathrm{NDVI} = \frac{\rho_{800} - \rho_{670}}{\rho_{800} + \rho_{670}} \tag{2}$$

where ρ_λ is spectral reflectance of the target at wavelength λ.

The upwelling target signal used in this example is synthesized from the downwelling solar irradiance measured with the SkySpec B hyperspectral radiometer [17] during clear sky conditions, with 36° solar zenith angle, and the top-of-canopy nadir reflectance of the birch stand from the database of optical and structural data of three mature hemiboreal forests at Järvselja, Estonia [20]. The stray light correction is applied separately to the measured downwelling irradiance spectrum and the synthesized upwelling target signal using the inverse matrix multiplication method described in [3]. Then, reflectance of the target is calculated as the ratio of the stray light-corrected upwelling and downwelling signals and the PRI and NDVI vegetation indices are calculated from the reflectance spectrum. Theoretically, PRI and NDVI can both vary between -1 and 1; however, in actual canopies, the range of PRI values is much smaller compared to that of NDVI values. To put the effect of FIA on calculated PRI and NDVI values into context, the absolute values are converted to relative units. The representative range of possible PRI and NDVI values is estimated from airborne top-of-canopy reflectance data measured with the UAVSpec spectrometer [21] at Järvselja, Estonia on July 5, 2010. The vegetation indices are calculated for 190 birch-dominated stands, which are larger than 0.5 ha and older than 5 years. For this representative case, PRI varies between -0.009 and -0.076, while NDVI values vary between 0.77 and 0.94. The calculated PRI and NDVI values after stray light correction are presented in Fig. 10; the results are shown in terms of the relative change in vegetation index with respect to the representative range, normalized to 1 at nominal FIA of 25°. Increasing the FIA by 1° in the range of 10°–40° changes the relative PRI value by 0.3%, which is an order of magnitude greater than the relative impact on NDVI.

V. Conclusion

We have shown in our study that the SLM of the Zeiss MMS 1 spectrometer depends on the illumination geometry. The stray light contribution and the width of the bandpass both increase with the illumination FIA, even outside of the nominal acceptance cone of the optical fiber. This should be considered when designing entrance optics for systems with fiber optic input, especially if the fiber is short.

Our results indicate that spectral stray light measurements performed with different setups give similar and repeatable results if the illumination beam geometry is similar. Given the fact that the SLM is necessary for removal of the stray light contribution from the measured signal, it is important to make sure that the conditions during stray light characterization match those during the target measurement.

The impact on the final data product of the illumination geometry used during stray light characterization depends on the target signal and the particular application. As demonstrated, in this paper by the example of NDVI and PRI vegetation indices, the relative impact can differ by an order of magnitude even for data products calculated from exactly the same target spectrum.

Although this study is limited to one particular model of spectrometer, the Zeiss MMS 1, and should not be generalized for all diode array spectrometers (or indeed for all individual instruments of this same model), it points out an important aspect of stray light characterization—the measured LSF may depend on illumination beam geometry.

Acknowledgment

The authors would like to thank C. Greenwell for her support with the STAIRS LabVIEW software and T. Goodman together with P. Miller for their technical review of this paper.

References

[1] G. R. Hopkinson, T. M. Goodman, and S. R. Prince, *A Guide to the Use and Calibration of Detector Array Equipment*, vol. 142. Bellingham, WA, USA: SPIE Press, 2004.

[2] H. J. Kostkowski, *Reliable Spectroradiometry*. La Plata, MD, USA: Spectroradiometry Consulting, 1997.

[3] Y. Zong, S. W. Brown, B. C. Johnson, K. R. Lykke, and Y. Ohno, "Simple spectral stray light correction method for array spectroradiometers," *Appl. Opt.*, vol. 45, no. 6, pp. 1111–1119, Feb. 2006.

[4] A. Coleman, R. Sarkany, and S. Walker, "Clinical ultraviolet dosimetry with a ccd monochromator array spectroradiometer," *Phys. Med. Biol.*, vol. 53, no. 18, pp. 5239–5255, 2008.

[5] H. Slaper, H. A. J. M. Reinen, M. Blumthaler, M. Huber, and F. Kuik, "Comparing ground-level spectrally resolved solar uv measurements using various instruments: A technique resolving effects of wavelength shift and slit width," *Geophys. Res. Lett.*, vol. 22, no. 20, pp. 2721–2724, 1995.

[6] S. W. Brown *et al.*, "Stray-light correction algorithm for spectrographs," *Metrologia*, vol. 40, no. 1, pp. S81–S84, 2003.

[7] S. Nevas, G. Wübbeler, A. Sperling, C. Elster, and A. Teuber, "Simultaneous correction of bandpass and stray-light effects in array spectroradiometer data," *Metrologia*, vol. 49, no. 2, pp. S43–S47, 2012.

[8] E. Torrecilla, S. Pons, M. Vilaseca, J. Piera, and J. Pujol, "Stray-light correction of in-water array spectroradiometers. effects on underwater optical measurements," in *Proc. OCEANS 2008.*, IEEE, Sep. 2008, pp. 1–5.

[9] S. G. R. Salim, N. P. Fox, W. S. Hartree, E. R. Woolliams, T. Sun, and K. T. V. Grattan, "Stray light correction for diode-array-based spectrometers using a monochromator," *Appl. Opt.*, vol. 50, no. 26, pp. 5130–5138, Sep. 2011.

[10] L. Ylianttila, R. Visuri, L. Huurto, and K. Jokela, "Evaluation of a single-monochromator diode array spectroradiometer for sunbed uv-radiation measurements," *Photochem. Photobiol.*, vol. 81, no. 2, pp. 333–341, 2005.
[11] H. Shen, J. Pan, H. Feng, and M. Liu, "Stray light errors in spectral colour measurement and two rejection methods," *Metrologia*, vol. 46, no. 1, pp. 129–135, 2009.
[12] A. Kreuter and M. Blumthaler, "Stray light correction for solar measurements using array spectrometers," *Rev. Sci. Instrum.*, vol. 80, no. 9, 2009.
[13] A. Barlier-Salsi, "Stray light correction on array spectroradiometers for optical radiation risk assessment in the workplace," *J. Radiol. Prot.*, vol. 34, no. 4, pp. 915–930, 2014.
[14] T. Seim and S. Prydz, "Automated spectroradiometer applying computer analysis of spectral data," *Appl. Opt.*, vol. 11, no. 5, pp. 1169–1177, May 1972.
[15] M. E. Feinholz *et al.*, "Stray light correction of the marine optical system," *J. Atmos. Ocean. Technol.*, vol. 26, no. 1, pp. 57–73, 2009.
[16] A. Mac Arthur, C. J. MacLellan, and T. Malthus, "The fields of view and directional response functions of two field spectroradiometers," *IEEE Trans. Geosci. Remote Sens.*, vol. 50, no. 10, pp. 3892–3907, Oct. 2012.
[17] J. Kuusk and A. Kuusk, "Hyperspectral radiometer for automated measurement of global and diffuse sky irradiance," *J. Quant. Spectrosc. Radiat. Transf.*, vol. 204, pp. 272–280, 2018, doi: 10.1016/j.jqsrt.2017.09.028.
[18] A. P. Levick *et al.*, "Spectral radiance source based on supercontinuum laser and wavelength tunable bandpass filter: the spectrally tunable absolute irradiance and radiance source," *Appl. Opt.*, vol. 53, no. 16, pp. 3508–3519, Jun. 2014.
[19] M. Talone, G. Zibordi, I. Ansko, A. C. Banks, and J. Kuusk, "Stray light effects in above-water remote-sensing reflectance from hyperspectral radiometers," *Appl. Opt.*, vol. 55, no. 15, pp. 3966–3977, 2016.
[20] A. Kuusk, J. Kuusk, and M. Lang, "A dataset for the validation of reflectance models," *Remote Sens. Environ.*, vol. 113, no. 5, pp. 889–892, 2009.
[21] J. Kuusk and A. Kuusk, "Autonomous lightweight airborne spectrometers for ground reflectance measurements," in *Proc. 2nd Workshop Hyperspectral Image Signal Process.: Evolution Remote Sensing.*, 14–16 Jun. 2010.

Joel Kuusk received the B.Sc., M.Sc., and Ph.D. degrees in physics from the University of Tartu, Tartu, Estonia, in 2003, 2005, and 2011, respectively.

Since 2006, he has been with Tartu Observatory (merged with University of Tartu in 2018), Tõravere, Estonia. His research interests include optical radiometry and vegetation remote sensing, particularly top-of-canopy spectral reflectance measurements above forests from low-flying helicopter. He has studied parameters of optical remote sensing instruments affecting the measurement results, e.g., temperature effects, stray light, nonlinearity, and angular effects.

Ilmar Ansko received the B.Sc. degree in physics in 1997 and the M.Sc. degree in physics, in 2005 from University of Tartu, Tartu, Estonia. Since 2003, he has been with Tartu Observatory (merged with University of Tartu in 2018), Tõravere, Estonia, where he is a Senior Engineer. He is highly experienced in optics and spectroscopy, optical radiometry, and related topics. He has designed and operated *in situ* observation systems for remote sensing of water and atmosphere.

Agnieszka Bialek received the M.Sc. degree in technical physics from Wrocław University of Technology, Wrocław, Poland, in 2003. Since 2012, she has been working toward the part-time Ph.D. degree in electrical engineering at the University of Surrey, Guildford, U.K., with the aim to establish SI traceability for satellite derived optical images, land and ocean, using vicarious calibration methodologies.

Since 2006, she has been with the National Physical Laboratory, Teddington, U.K. Her scientific experience is related to optical measurements including absolute radiometric calibration and instruments characterization as well as data modeling. Her current research interest includes uncertainty reduction in earth observation by implementation of rigorous SI traceability.

Riho Vendt received the B.Sc., M.Sc., and Ph.D. degrees in physics from the University of Tartu, Tartu, Estonia, in 1994, 2008, and 2013, respectively.

He is highly experienced in quality assurance of tests and measurements. He has worked almost 20 years for the National Metrology Institute of Estonia (Metrosert, 1994–2013) being responsible for the national standards for thermometry (2004–2012). He was a member of the consultative committee for metrology at the National Accreditation Board (2000–2013), a member of the TC-Therm (Technical Committee for Thermometry) at EURAMET (European Collaboration in Measurement Standards) as the National representative for Estonia (2002–2013). He has been an active assessor of quality management systems since 2004. He is the Head of laboratories, Tartu Observatory, University of Tartu.

Nigel Fox received the B.Sc. degree in astronomy and physics and the Ph.D. degree in physics, for work undertaken at the National Physical Laboratory (NPL) dissertation entitled "The Absolute Measurement of Spectral Radiant Power," from University College London, London, U.K., in 1981 and 1997, respectively.

Since 1981, he has been with the NPL (the U.K. national standards Laboratory), Teddington, U.K., where he is currently an NPL Fellow and Head of Earth Observation. His research efforts have been largely concerned with the realization of primary radiometric scales and methods to improve their dissemination. This has largely been focused on the development and use of detectors and detector-based techniques for optical radiation measurement. He has authored or coauthored more than 120 papers.

Dr. Fox has been an active participant of the Committee on Earth Observation Satellites Working Group on Calibration and Validationv and associated subgroups since 1996 and Chair of its Infrared, Visible, and Optical Sensors subgroup since 2006.